JOURNAL OF MECHANICAL ENGINEERING AND SCIENCES
ISSN: 2289-4659 e-ISSN: 2231-8380
VOLUME 17, ISSUE 1, 2023, 9324 – 9337
DOI: https://doi.org/10.15282/jmes.17.1.2023.3.0737

RESEARCH ARTICLE

Evaluation of welding-induced residual stress and distortion in A-TIG welding of duplex stainless steel

A. Siyavoshi[1,*], S. Shakhesi[1,2], M. Reza Afshar[1,3], M. Hashemzadeh[4] and M. Noghabi[5]

[1] Department of Materials Engineering, Science and Research Branch, Islamic Azad University, 1477893855, Tehran, Iran
[2] Institute of Mechanics, West Fal Asiri Street, 71555414, Shiraz, Iran
[3] Department of Advanced Materials & Processing, Research and Development of Engineering Materials Research Center, Science and Research Branch, Islamic Azad University, 1477893855, Tehran, Iran
[4] Centre for Marine Technology and Ocean Engineering (CENTEC), Instituto Superior Técnico, Universidade de Lisboa, 1049001, Portugal
[5] Department of Mechanical Engineering, Amirkabir University of Technology, 1591634311, Tehran, Iran

ABSTRACT - Applying non-uniform heat in welding causes residual stress and distortion, which affects the life of components. In the present study, the residual stress and distortion of Duplex 2205 stainless steel in A-TIG welding were investigated numerically and experimentally. The optimal welding parameters for highest penetration depth in welded samples were obtained experimentally. Uncoupled thermal-mechanical analysis using ABAQUS 2017 software has been done. Goldak's parameters were measured by empirical tests. The results include simulation diagrams of four samples consisting of the optimal sample without flux powder and three samples with the highest penetration depth. The simulation results show that the sample without flux has a higher maximum temperature and lower welding-induced distortions. The efficiency used in this research changes using and not using powder; it is concluded that, in similar conditions in A-TIG welding, fewer values of parameters are needed to achieve the appropriate result comparing conventional TIG. The efficiency of workpieces with flux should be considered about 20% lower to have similar results to the conventional TIG. The numerical modeling results showed a good agreement with experimental data both for temperature distribution and welding-induced residual stress and distortion. The distortion in the pieces with conventional TIG welding has increased to 11% at the farthest point from the welding line. The error obtained from comparing the results in residual stress is between 12 and 34%.

ARTICLE HISTORY
Received : 23rd Nov. 2022
Revised : 12th Feb. 2023
Accepted : 24th Feb. 2023
Published : 23rd Mar. 2023

KEYWORDS
Welding
Residual stress
Distortion
Welding simulation
A-TIG welding
Duplex stainless steel

1.0 INTRODUCTION

Gas Tungsten Arc Welding or Tungsten Inert Gas is one of the important melting arc welding processes [1]. It is highly regarded for its advantages, such as the high quality of the weld, its cleanliness, and better heating than peer-to-peer processes [2]. This welding has wide applications in modern technologies and industries [3]. Also, the important influencing parameters investigated in it are travel speed, intensity of electric current and flow rate of shielding gas [4]. The significant limitation of TIG process is the low penetration depth of the welding [5]. In order to overcome this problem, the activated TIG welding (A-TIG) has been developed [6]. In this method, with a mixture of active powder and solvent liquid, a thin layer of paste is applied to the workpiece. As a result of this process and changes in the plasma column and forces inside the molten pool, the penetration depth increases up to three times [7]. A number of features in the A-TIG method have been reported in some previous work. Unni et al. [8] focused on microstructural changes in A-TIG welding. They concluded that microstructural changes were due to the amount of oxygen in the weld as well as the surface tension temperature coefficient. The shape of the welding pool is predicted, and the optimal number of effective parameters is obtained. Kumar et al. [2] performed tensile and impact tests of active flux welding in steel specimens by implementing experimental and simulation methods. These kinds of tests are used to determine variables related to mechanical properties and show the reaction of materials to the application of load. Furthermore, they are essential in maintaining human health and preventing financial loss. Tathgir et al. [9] experimentally studied the effect of different fluxes in A-TIG welding on duplex stainless steel. They evaluated the amount of available oxygen, the factors that cause cracks, the growth of dendrites as well as the factors that create the depth of penetration in A-TIG welding. Unni et al. [10] performed a three-dimensional analysis of velocity and thermal fields. The aim of this study was to determine the amount of oxygen required to complete the reverse Marangoni flow and its effect on the weld dimensions. In general, the model used for different amounts of oxygen has a good prediction. This model also determined the amount of oxygen required for maximum penetration depth.

During welding, regional and non-uniform heat is applied to the piece, and in the cooling stage, non-uniform contractions occur that cause induced residual stress and distortion. These residual stress and distortion induced by welding reduce the strength of welded structures [11, 12]. Since workpieces' physical and mechanical properties are

***CORRESPONDING AUTHOR | A. Siyavoshi** | ✉ a.siyavoshi@srbiau.ac.ir

affected during welding operations, residual stress and distortion reinforce the creation and expansion of various types of cracks and fractures [13]. Preventing the growth and repair of structures requires a lot of money and time. Therefore, welding-induced residual stress and distortion are two significant effects of welding processes that may cause problems in the later stages of operation. For example, residual stress can reduce useful life, and distortion can cause dimensional mismatch and service problems, especially in essential industries [13, 14]. Therefore, investigating the residual stress and distortion induced by welding is important, and many researchers have focused on this subject in recent decades [15-20].

Many studies about stress and distortion have been conducted in recent years. Chen et al. [21] numerically and experimentally investigated the welding-induced residual stresses of a nickel-based superalloy. Residual stresses were analyzed in different directions, and the model's reliability was validated. Sun et al. [22] have investigated the effect of geometric parameters of heat source and arc efficiency on mechanical and thermal properties of welding. In this research, analyzes have been performed by calibrating the efficiency and parameters of the heat source. Welding parameters had little effect, but arc efficiency significantly affected the results. Vasantharaja et al. [18] reviewed the welded joints of 316LN stainless steel sheets produced by multi-pass TIG and A-TIG processes. It was concluded that A-TIG welding shows less residual stress and distortion due to the absence of filler metal, direct edge preparation, single-pass, and more concentrated heat source. Zubairuddin et al. [23] investigated residual stress distribution and distortion of modified 9Cr-1Mo steel sheets using thermal-mechanical modeling. They compared the thermal history, residual stress, and distortion in the simulated samples by measuring them. Ahmad et al. [14] performed a numerical analysis of residual stress and distortion of two-pass TIG welding of 2219 aluminum sheets by combining ABAQUS and FORTRAN. The Goldak heat source model was implemented by the DFLUX subroutine. They concluded that thermo-mechanical using finite element method implementing double ellipsoid heat source are reliable. Farhang et al. [24] have investigated the effect of important parameters of friction stir welding method on residual stress. In this welding method, the simulation has acceptable results compared to the laboratory conditions, and in addition, the optimal conditions for the parameters have been obtained. Gao et al. [25] performed finite element simulation based on microstructure to investigate deformation of Duplex 2205 steel welded by TIG. Strain behavior and deformation using the finite element method have been investigated. In the obtained results, with the change of morphology, the strain microstructure is dispersed non-uniformly, which causes the error to occur simply. Also, the ratio of phases in duplex steel is different in welding and base metal, and changing them in the strain creation in each region is effective. Hashemzadeh et al. [26] have also studied the thermal and mechanical analysis of butt-welding of thin plates. They have obtained an equation for estimating residual stress and distortion. This research has been highly accurate in validating the results.

Recently, Duplex steels have been designed to provide higher strength and better corrosion resistance. These types of steel have two-phase of ferrite and austenite. Appropriate ratios of phases must be obtained because their mechanical properties and corrosion resistance are derived mainly from the balance of these two phases. With a higher ferrite phase ratio, the corrosion resistance will be reduced. If this ratio is low, it reduces the strength and resistance to crack foundations [25, 27]. A proper phase ratio maintains steel properties at low temperatures [9]. These steels have better weldability and hardness than ferritic steels and higher stress resistance against cavities and cracks than austenitic steels [28]. The various applications of these steels are due to their microstructure and their excellent properties in corrosion resistance and weldability [29].

As mentioned earlier, some research has been conducted based on residual stress and distortion simulation on duplex Stainless steel. Considering wide applications of duplex stainless steel for biomedical [30], petrochemical [9], automobile structural applications [31], marine equipment structures, concrete structures in oil and gas pipelines [32, 33], etc; further investigations are needed to study various aspects of micro and macro structures of these kinds of steels. In this study, residual stress and distortion in A-TIG welding of Duplex 2205 steel are evaluated by an uncoupled finite element model with ABAQUS, and the accuracy of the corresponding results is studied. To verify the results, a comprehensive experimental study is performed. In this regard, to record the thermal history, a type K thermocouple is used. Distortion is measured by CMM machine and residual stress by hole drilling method. The required variables to simulate Goldak's heat source in FEM are obtained from the samples in a metallographic test. Furthermore, the chemical composition of the steel is determined by Spark Emission Spectroscopy.

2.0 NOMENCLATURE

ρ	Materials density, $[g/mm^3]$	C_p	Specific heat capacity, $[J/g\,℃]$
T	Current temperature, [℃]	Q	Internal heat generation rate, $[W/mm^3]$
x, y, z	Coordinates in the reference system, [mm]	t	Time, [s]
K	Thermal conductivity, $[W/(m\ ℃)]$	q_c	Convection heat losses, $[W/mm^2\ ]$
h_f	Film coefficient for convection, $[W/(mm^2\ ℃)]$	T_{sur}	Surface temperature, [℃]
T_0	Ambient temperature, [℃]	q_r	Radiation heat losses, $[W/mm^2\ ]$
σ	Stefan–Boltzman constant, $[W/(mm^2\ ℃^4)]$	ε	Emissivity
α_h	Heat transfer coefficient, $[W/m^2]$	ε^{total}	Total strain
ε^e	Elastic strain	ε^p	Plastic strain
ε^{th}	Thermal strain	ε^v	Volumetric change strain

x', y', z'	Local coordinates of the double ellipsoid, [mm]	f_f	The fraction of the heat deposited in the front parts, [mm]
f_r	The fraction of the heat deposited in the rear parts, [mm]	a	The width of the molten zone, [mm]
b	The depth of molten zone, [mm]	c_f	The front semi-axis of the ellipsoid, [mm]
c_r	The rear semi-axis of the ellipsoid, [mm]	Q_w	Heat input, [W]
U	Voltage, [V]	I	Current intensity, [A]
η	Welding efficiency, [%]		

3.0 EXPERIMENTAL PROCEDURE

The chemical composition and type of steel have been investigated by experiments. The specimens' dimensions were defined because the primary purpose of the experiment was to obtain the optimal A-TIG welding conditions and the dimensions of the welding pool. The material of Duplex 2205 ASTM A240 stainless steel was prepared with a chemical composition in Table 1 and cut into 100 x 100 x 8 mm pieces.

Table 1. Chemical composition of Duplex 2205 stainless steel (wt%)

C	Si	Mn	P	S	Cr	Mo	Ni	Al
0.02	0.45	1.2	0.02	0.003	23.0	3.5	5.9	0.004
Co	Cu	Nb	Ti	V	W	N	Fe	
0.04	0.03	0.01	0.016	0.06	0.02	0.18	Base	

Welding conditions of the studied samples, including current intensity, traveling speed, electrode tip angle, and activating powder, are presented in Table 2. First, the flux powder is dissolved by Acetone and made into a uniform solution. After applying the powder according to Figure 1 which shows the uniformity of the applied layer and preparing the samples, welding was performed. Table 3 shows the properties related to the process parameters of the TIG welding method. Considering similar investigations to the present study [5, 34-36], an approximate range of numbers related to variable welding conditions were identified. Welding was done by Khazar Transfo KTTIG 350A AC / DC machine. The results of welding pool characteristics obtained from the prototypes were compared, and 23 cases were considered. Given that the aim of this research is to overcome the limitation of the TIG welding method, the optimal sample is the specimen with full penetration depth and smaller weld width. Therefore, specimens with active flux were selected from 23 samples by changing the conditions mentioned to achieve samples with greater penetration depth. The specimen without flux is also included for better comparison.

Table 2. Welding parameters of samples

Sample Name	Powder	Current Intensity (A)	Traveling Speed (mm/min)	Tip Angle (°)
W	-	200	78	60
A	SiO_2	200	78	45
B	SiO_2	200	78	60
C	$75\%SiO_2+25\%TiO_2$	200	78	60

Figure 1. Sample with applied layer of flux powder

Table 3. Process fixed welding parameters for all of the experiments

Parameter	Value
Electrode Diameter	2.4 mm
Electrode Type	EWTh-2
Arc Gap	3 mm
Shielding Gas	Pure Argon
Gas Flow Rate	15 lit/min

Evaluation of thermal simulation results was performed by measuring temperature changes during the welding process using a K-type thermocouple installed in the position shown in Figure 2. Temperature changes were recorded using the Center 309 Data Logger thermometer with an accuracy of 0.1 ℃.

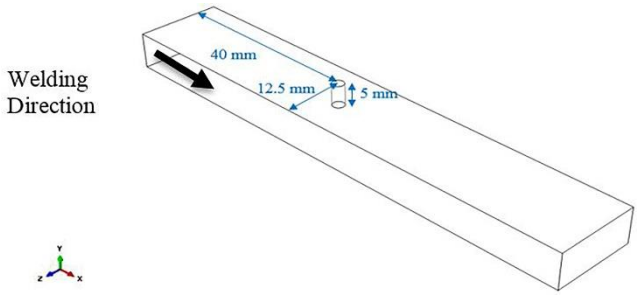

Figure 2. Thermocouple connection point coordinates

After preparing all workpieces and performing welding, the selected samples are used to obtain the characteristics of the welding pool. After this step, the experiments are repeated with similar samples to perform final tests and check the thermal history in the specified conditions. In the next step, the specimens are polished by a magnetic grinding machine to eliminate surface imperfections and prepared for distortion and residual stress tests. Figure 3 is related to the distortion measuring test with a coordinate measuring machine (CMM). In this measurement, the weld's centerline is considered a reference, and the coordinates of the other points are measured relative to this line.

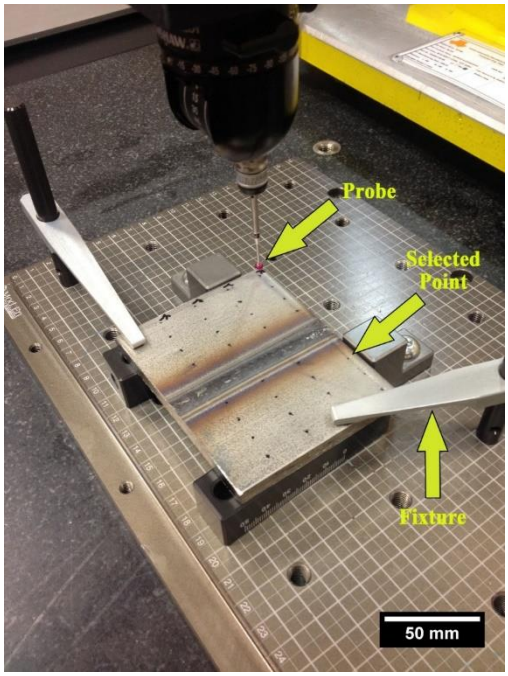

Figure 3. Distortion measurement by coordinate measuring machine

Figure 4 shows one of the samples tested for residual stresses and how strain gauges are installed in this test. As mentioned earlier, the method of measuring residual stress is the hole drilling method. In this method, samples are evaluated according to ASTM E-837 standard.

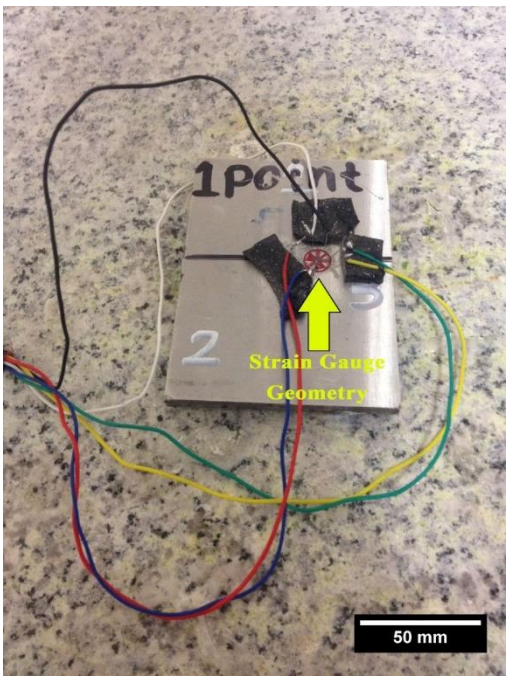

Figure 4. Residual stress measurement and strain gauges

4.0 FINITE ELEMENT ANALYSIS

To simulate welding, Abaqus finite element software is used, and by performing transient thermo-mechanical analysis, temperature field and welding-induced residual stress and distortions are calculated.

4.1 Workpiece Geometry, Mechanical Boundary Conditions, and Mesh

Samples geometry is shown in Figure 5. Due to the symmetry in the welding as well as reduction in analysis time, half of the sample is simulated.

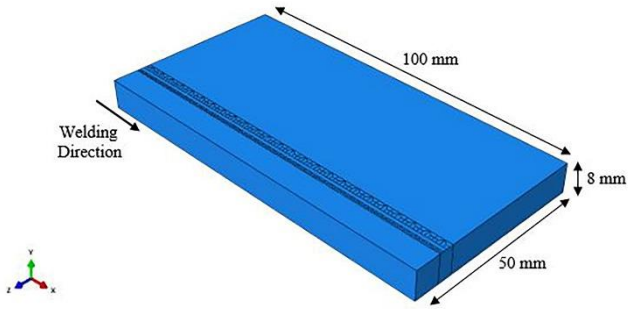

Figure 5. Geometric model of the welded workpiece

The mesh of specimens is shown in Figure 6. Also, the weld area, which was separated in the geometry section, is considered finer mesh for more accurate results. DC3D8 type elements are used for thermal analysis, and C3D8R type is used for mechanical analysis which are, respectively, the 8-node linear cubic element suitable for heat transfer analysis and the 3-dimensional 8-node cubic element with a reduced formulation. In this research, it is assumed that the model is symmetrical; therefore, the plate center of the sample is considered symmetric due to the z-axis. To prevent specimen movement, a point at the beginning of the weld line is considered as a reference point, and an end point is limited in the vertical direction, which indicates the boundary conditions in mechanical analysis. The specified path as a dotted line in the figure is the source of extracting the results to simulate distortion and residual stress.

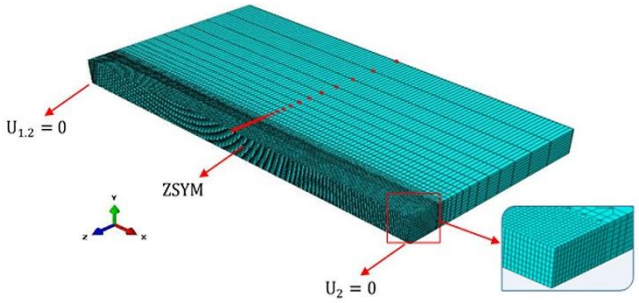

Figure 6. Mesh, mechanical boundary conditions and extraction path of results in sample geometry

The sensitivity analysis results to mesh number are presented in Figure 7. A sample with 61,600 elements and 71,820 nodes was considered. The smallest mesh size in the weld area is 0.25 x 0.49 x 1 mm. In parts further from the weld, due to the lower sensitivity of the mesh results, the mesh is a single bias type. Bias mesh is applied because the mesh, which is further away from the weld and has less impact on the results, is more extensive and thus reduces the run time. The transient mesh also creates the connection between the meshes of two areas.

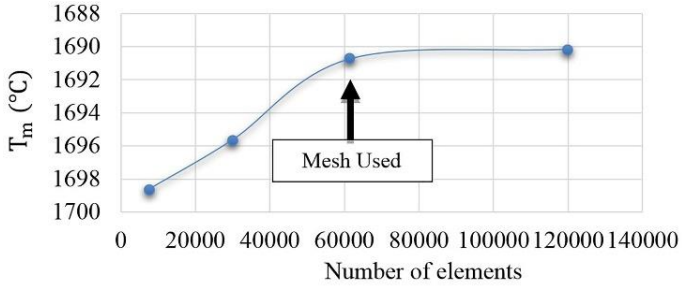

Figure 7. Mesh sensitivity analysis diagram

In this study, finite element analysis was accomplished by the uncoupling method. In the uncoupling method, first, thermal analysis is performed, and then the temperature obtained from each node is used as the input for mechanical analysis. Both analyses were implemented by the implicit method.

4.2 Workpiece Properties

For making the analysis, the physical and thermal properties of the pieces will be required, which are present in Figure 8. The extraction was done through JMatPro v.7.0 software and considering the work reported by [37]. JMatPro is a software that calculates the properties of the samples, including thermal, mechanical, solidification, phase transformation, etc., by specifying the chemical composition as input. After measuring the chemical composition elements, these properties are entered into the software, and the properties of the sample are obtained. These temperature-dependent properties have been incorporated into Abaqus software for more accurate simulations.

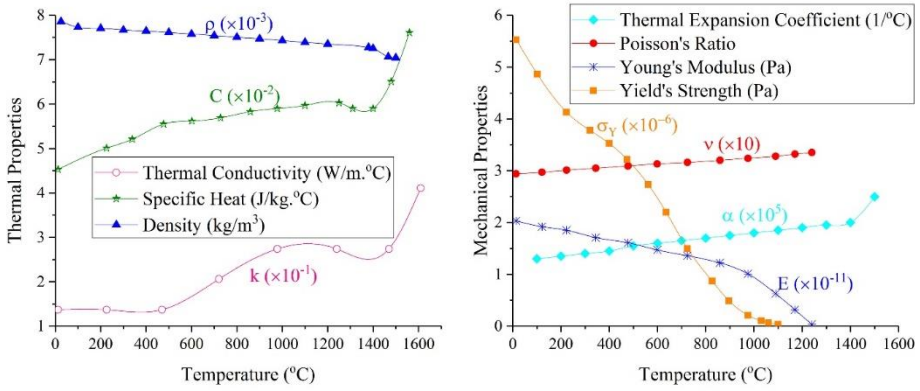

Figure 8. Temperature-dependent properties of Duplex 2205 stainless steel

The latent heat of steel, the temperature of the solidus, and the temperature of liquidus are presented in Table 4. Latent heat is used to induce solidification behavior.

Table 4. Properties of solidification behavior in 2205 steel [29]

Property	Value
Latent heat of fusion (**kJ/kg**℃)	500
Solidus temperature (**℃**)	1385
Liquidus temperature (**℃**)	1500

4.3 Mechanical, Thermal Analysis, and Thermal Boundary Conditions

In finite element analysis, the used equations for thermal analysis are summarized as follows [12, 15]

$$\text{Energy conservation law: } \rho C_p \frac{\partial T}{\partial t} = \frac{\partial}{\partial x}\left(k\frac{\partial T}{\partial x}\right) + \frac{\partial}{\partial y}\left(k\frac{\partial T}{\partial y}\right) + \frac{\partial}{\partial z}\left(k\frac{\partial T}{\partial z}\right) + Q \tag{1}$$

$$\text{Convection heat loss: } \quad q_c = -h_f(T_{sur} - T_0) \tag{2}$$

$$\text{Radiation heat loss: } \quad q_r = -\varepsilon\sigma(T_{sur}^4 - T_0^4) \tag{3}$$

During welding, the workpiece is strained as a result of heat, and the total strain is defined as the sum of each strain component alone:

$$\varepsilon^{total} = \varepsilon^e + \varepsilon^p + \varepsilon^{th} + \varepsilon^v + \varepsilon^{tr} \tag{4}$$

As regards the stainless steel, the phase transfer strain ε^{tr} and the volume change strain ε^v do not have a significant effect; then they are ignored in the calculation of strain so that the total strain will be calculated from Eq. (5) [14, 15]:

$$\varepsilon^{total} = \varepsilon^e + \varepsilon^p + \varepsilon^{th} \tag{5}$$

In the present work, instead of heat loss formulas, combined thermal boundary conditions proposed by Brickstad and Josefson [38] are used for all surfaces except the symmetrical surface in the middle of the specimen, which is calculated for convection and radiation. The expression of the results for the heat transfer coefficient related to temperature, α_h, is given by Eqs. (6) and (7) depending on the temperature of the workpieces. Also, the initial temperature of the piece was considered to be 25℃.

$$\alpha_h = 0.0668 \cdot T \ \ \mathrm{Wm^{-2}.℃} \qquad 0 < T < 500\ ℃ \tag{6}$$

$$\alpha_h = 0.231 \cdot T - 82.1 \ \ \mathrm{Wm^{-2}.℃} \qquad T > 500\ ℃ \tag{7}$$

User-defined subroutines are used to code heat transfer analysis to model thermal flux source, radiant, and convection boundary conditions. The power distribution in the Goldak method combines two equations for two ellipses:

$$Q(x'.y'.z'.t) = \frac{6\sqrt{3}f_r Q_w}{abc_r\pi\sqrt{\pi}} e^{-3\left(\frac{x}{a}\right)^2} e^{-3\left(\frac{y}{b}\right)^2} e^{-3\left(\frac{z}{c_r}\right)^2} \tag{8}$$

$$Q(x'.y'.z'.t) = \frac{6\sqrt{3}f_f Q_w}{abc_f\pi\sqrt{\pi}} e^{-3\left(\frac{x}{a}\right)^2} e^{-3\left(\frac{y}{b}\right)^2} e^{-3\left(\frac{z}{c_f}\right)^2} \tag{9}$$

f_f and f_r factors define the heat fraction in the front and rare ellipses, respectively, which reaches $f_f + f_r = 2$. Table 5 contains the values a, b, c_f and c_r for all four samples, which are derived from the experimental tests and metallographic pictures. Finally, f_f and f_r factors were defined as 0.6 and 1.4, respectively [39]. Figure 9 also shows the welding pool and the required parameters in the formulas.

Table 5. Goldak parameters extracted from experimental tests

Sample Name	Goldak's Parameters (mm)			
	a	b	c_f	c_r
W	6.92	4.35	4.5	10.22
A	4.7	7.75	4.0	12.31
B	4.86	8	4.1	12.64
C	5	8	3.33	11.14

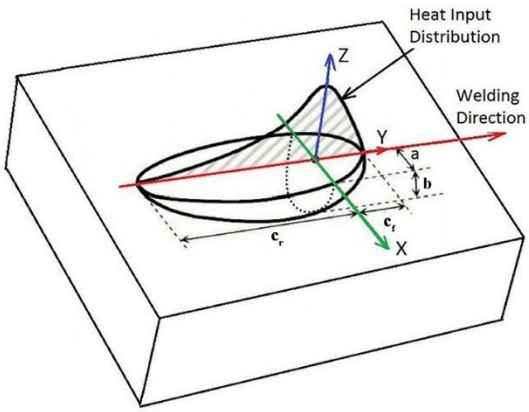

Figure 9. Goldak parameters in the weld pool [39]

The heat input in Goldak double ellipsoidal formulas is the same as the welding heat input calculated from Eq. (10).

$$Q_w = U.I.\eta \tag{10}$$

In the present work, the current intensity is constant part of the experiment. However, the voltage is different with the conditions that the average voltage measured for the samples is as described in Table 6. According to TIG welding, the efficiency coefficient has different ranges for different processes, which is considered almost 0.7 in this analysis [40, 41]. Simulation of all four samples (W, A, B and C) has been done according to Eqs. (8), (9) and (10), fixed parameters and parameters specified in Tables 5 and 6.

Table 6. The average voltage of the welding machine

Sample Name	Voltage (V)
W	17.05
A	18.43
B	18.83
C	18.60

5.0 RESULTS AND DISCUSSION

5.1 Measurement of Thermal History

Figure 10 shows the experimental measurement results for the temperature distribution of four samples. It is observed that in the graph related to the sample without flux, the maximum temperature is higher than the other samples. The reasons can be explained by the fact that from one side, there is no thermal concentration in the sample without flux, and heat is dissipated, so the points at a distance from the center of the weld absorb a higher temperature. On the other hand, in the specimens with flux, heat is used to eliminate flux, and as a result, the maximum temperature is reduced.

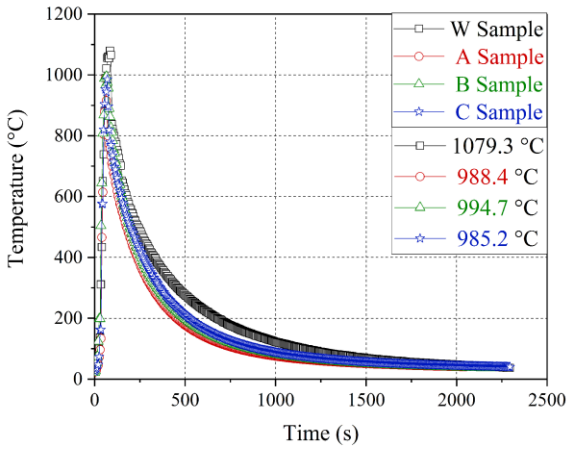

Figure 10. Experimental measurement of the thermal history and maximum temperature of samples

The variations of efficiency used in the heat input formula are shown in Table 7. In this research, all input dimensions and parameters in the subroutine file and software have been measured, to achieve thermal analysis and temperature history of the samples, the only parameter that can be changed is efficiency [39]. From Table 7 it is observed that the flux powder has caused a significant change in the amount of efficiency. It can be explained by the fact that the input parameters affect each other; a parameter such as penetration depth covers a more significant portion. Given that all of these numbers are used in the double ellipsoidal formula, more amount of each makes the numerical value of the lower efficiency is required. Comparing the values, the efficiency for workpieces with flux should be considered to be about 20% lower to have the same results as the conventional TIG. A comparison of the three samples with the powder shows that the numbers are close to each other however some differences occur. As mentioned earlier, the reason can be expressed several parameters are used in calculations that affect the overall result, including the numbers in Goldak's formula, voltage, current intensity, and efficiency.

By considering the values obtained in Table 7, sample A has all the optimal conditions and also has higher value parameters among the samples with flux, so it has low efficiency. Among the other two samples, sample B in b_f and b_r and sample C in the depth of penetration, weld width, and voltage have more values, the result of which seems to have reduced the required efficiency of this sample. This means that under the same conditions in A-TIG welding, smaller values of parameters are required to achieve results than conventional TIG welding.

Table 7. Variations in simulation efficiency by adding flux

Sample Name	Efficiency (%)
W	70.45
A	55.85
B	55.36
C	55.61

5.2 The Results of Distortion Simulation

The results of distortion simulation in the direction of thickness for all samples are given in Figure 11. In the welding area as well as in the surrounding areas, which have higher temperatures, the amount of displacement has increased significantly. Considering Figure 12 which is shown in part (a) before welding and part (b) after welding, the reason is that in addition to the expected displacement, the sample has additional distortion due to the presence of very high thermal flux in the target areas, and according to the dimensions of the sample displacement that the values are in the range of 0.01 mm, it is very high.

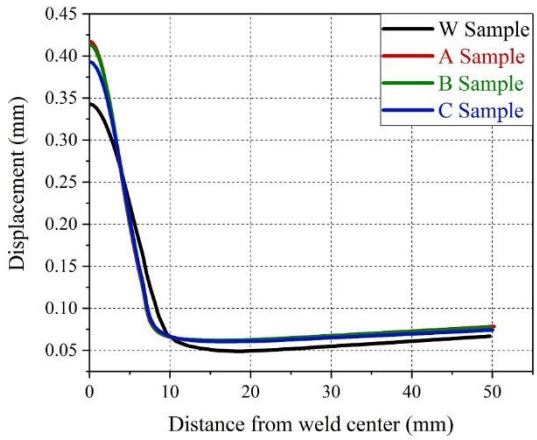

Figure 11. Distortion diagram extracted from software for all samples

Considering the diagrams of the samples in the part where the displacement is closer to reality, it is observed that the sample without flux has less distortion than the other samples. It could be possible to justify this by considering the factors affecting the distortion, including the number of passes, welding speed, the relative penetration, the shape, the dimensions of the weld, and the heat input that can be checked [14]. In welding without flux, the penetration is the lowest, shallow welded shape, and this welding has less distortion even with higher heat input comparing the samples with flux. Nevertheless, the results differ from the results of other studies in experimental measurements [5, 7]. Due to the factors affecting the distortion which are mentioned earlier, it is possible that the heat input and its uniformity, as well as the number of passes, play a significant role and as regards the heat dissipation is more uniform in the whole piece without flux. Therefore, all weldments are single-pass, less distortion has occurred.

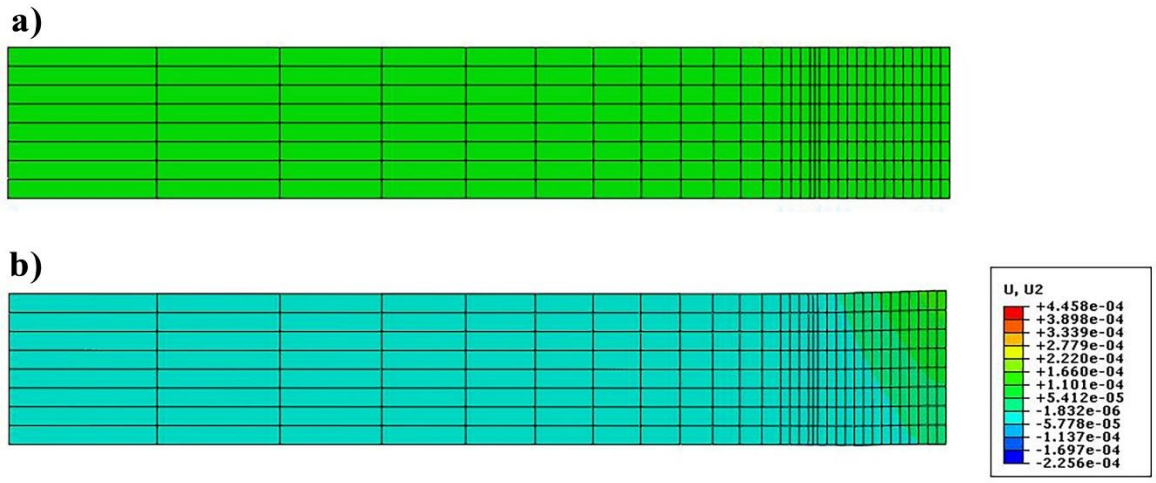

Figure 12. Cross-sectional geometry of sample: a) before and b) after mechanical analysis

5.3 Thermal Analysis Validation

Figure 13 depicts a comparison of results and the experimental measurement of temperature history. These diagrams also show that the graphs are fully agreed upon during welding, but there are differences in the cooling process. This difference can be attributed to the thermal loss, the corresponding errors, and the simplifications considered in it [12]. Another noteworthy and important point is that all samples with flux create a cooling rate diagram with a lower slope compared to the conventional TIG sample. Ramkumar et al. [42] mentioned the reason which has a slower cooling rate in this process. This low rate also reduces the difficulty of austenite formation and increases the possibility of improving the ratio of ferrite to austenite [34, 39].

On the other hand, according to the research results of Zubairuddin et al. [23] that the cooling rate and the heating rate are different due to the heat source model of the double ellipsoidal, therefore this difference may indicate a variation in the parameters of the double ellipsoidal of these welds.

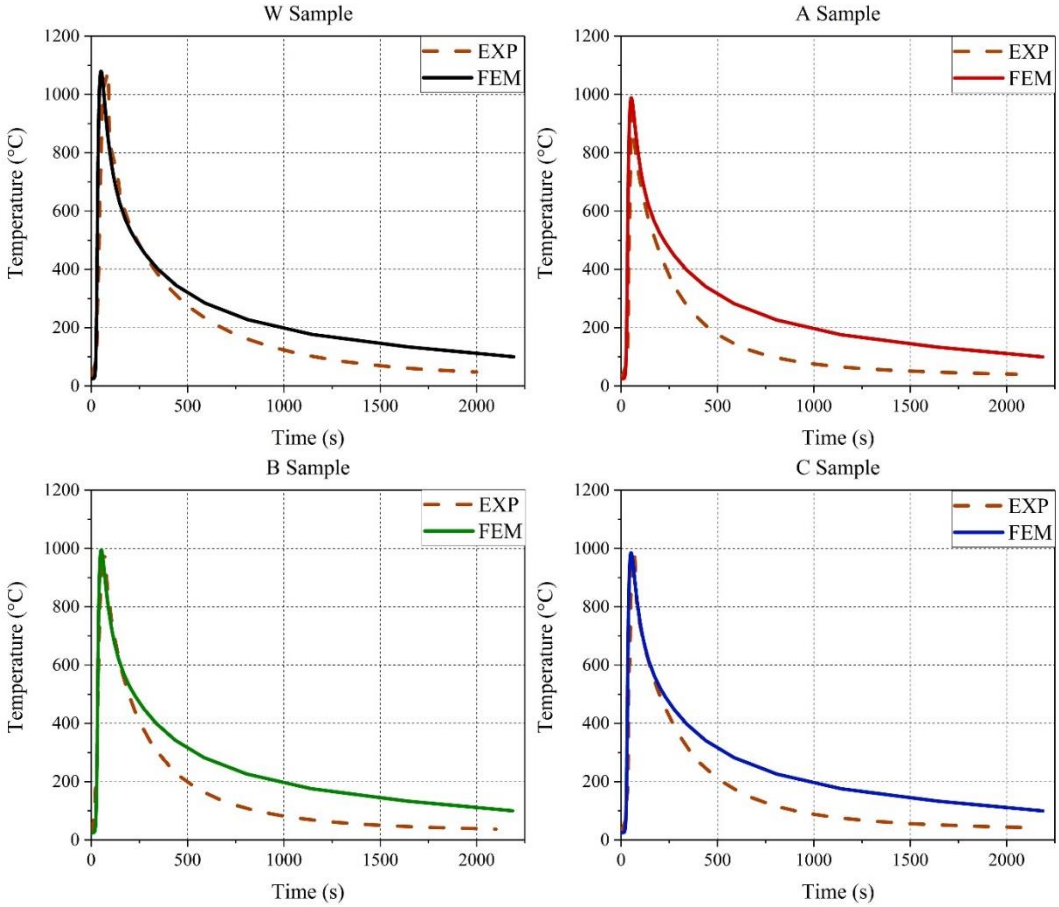

Figure 13. Comparison between experimental and simulation thermal history

5.4 Distortion Simulation Validation

In Figure 14, average values of distortion measured experimentally are compared with simulation results. The results are generally acceptable, but there is some discrepancy in the results, and since the simulation is close to the standard deviation in the measurement of points in the whole sample, this is acceptable. However, in general, the deviation can be attributed to various factors, such as the fact that the conditions in the simulation are ideal, but there can be some errors in the actual case. Also, the measurement of welding method parameters has also been done manually, so it would be expected for some errors to occur.

In the results of the simulated distortion change process, appropriate compliance with experimental results is observed. The difference may be since the measuring device in this experiment is a precise and sensitive device [26], and if there is the slightest difference in dimensions, even very small, measurements are made, which may be the reason for the difference in this research. Another important point that can be mentioned is that by comparing the experimental results, the distortion is higher in the workpiece without flux, which is calculated to be about 11% at the farthest point from the welding line. The reason for this phenomenon can be explained by the factors affecting the distortion, the most important is the weld metal volume, which determines the depth of penetration, shape and dimensions of the weld.

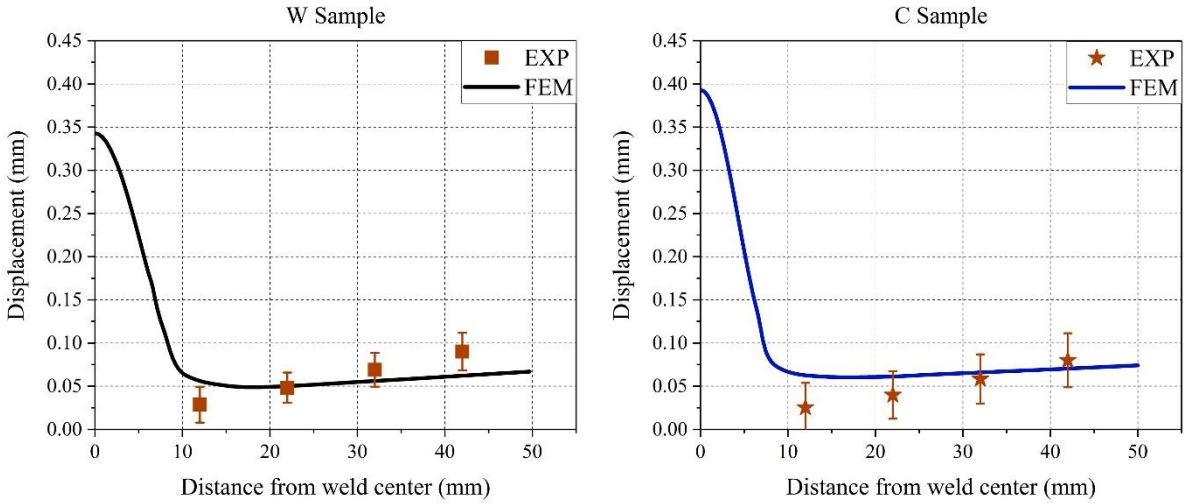

Figure 14. Comparison between experimental and numerical of two samples displacement

5.5 Residual Stress Simulation Validation

Figure 15 represents the residual stress diagrams of the experimental and numerical to validate the simulation. As stated in other studies [9, 12], the simulated residual stress in the samples is close to the base metal yield stress. The yield stress is initially tensile in the weld line area and becomes compressive stress as it moves away from the weld line [14]. This is the general basis of stress in welded workpieces. There are differences in the results of experimental and simulation. The causes of these differences in examining, the measured values in the experiment are close to each other, and knowing that many factors including experimental and simulation errors in creating differences may be considerable. Simulation is a method in which all conditions exist ideally, and errors are not considered. There are also several simplifications for simulation, so the simulation numbers show a different value [21, 43].

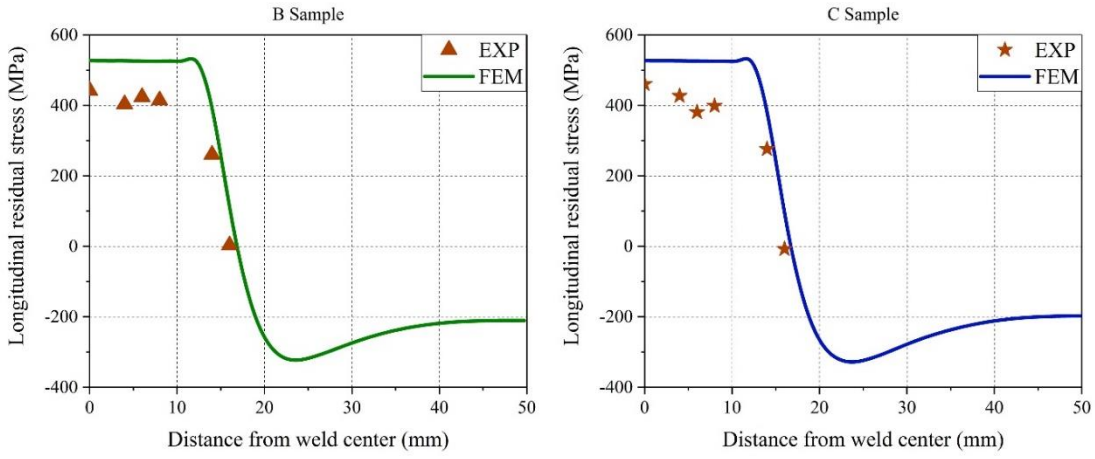

Figure 15. Comparison between experimental and numerical of two samples residual stress

On the other hand, practical experiments should be considered for their errors [44], sensitivity of strain gauges, and errors related to the dimensions of the cavity and surface conditions and the sample itself, for example, smoothness and leveling of the surface and alignment of strain gauges. This is the reason for the decrease in values. Kandil et al. [45], in their report, point to these differences. However, in general, the simulation and practical experiment results are the same as the process reported in other studies [11-13, 17, 18, 23]. The diagrams show the expected trend that occurs in welded pieces. The calculated error between simulation and experimental test is in the range of 12 to 34%.

6.0 CONCLUSION

In the present study, the possibility of simulating residual stress and distortion in duplex 2205 stainless steel A-TIG welding by Abaqus software has been considered. The hole-drilling method for residual stress measurement, the CMM device for measuring the distortion related to the specimens, and the thermometer data logger is used for the thermal history in laboratory measurements. The measurement results were reported in the history of temperature and distortion and compared with the validation simulation results. In the stages and results of this experiment, conclusions have been obtained, the most important of which can be mentioned in most of the following cases:

- Comparing simulated thermal histories of samples, the sample without flux has a higher maximum temperature. The difference is due to the lack of thermal concentration in the sample without the flux, as well as the presence of the flux itself, which causes heat loss in reaching the workpiece.
- Comparing simulated distortion distributions of samples, the sample without flux has less distortion. It is because of single-pass, which does not experience a large thermal cycle, and the heat input at which the thermal distribution is more uniform.
- The efficiency used in this research using powder and not using it is different; as a result, in similar conditions in A-TIG welding, fewer values of parameters are needed to achieve the appropriate result than conventional TIG. The efficiency for workpieces with flux should be considered about 20% lower to have similar results to the conventional TIG workpieces.
- Performed thermal analysis is in good agreement with the experimental measurement. The difference can be considered a result of heat loss and the simplification considered in the simulation.
- In the simulation of distortion and validation, acceptable results have been obtained. The differences can be due to the manual measurement of Goldak parameters and the high accuracy of the distortion-measuring device. The distortion in the pieces with conventional TIG welding has increased to 11% at the farthest point from the welding line.
- In residual stress simulation and its validity, the results show the expected trend that occurs in welded pieces. The difference is also due to errors in the experiment. The error between simulation and experimental test is in the range of 12 to 34%.

6.0 REFERENCES

[1] E. Ahmadi, A. R. Ebrahimi, and R. Azari Khosroshahi, "Welding of 304L stainless steel with activated Tungsten inert gas process (A-TIG)," (in english), *International Journal of Iron & Steel Society of Iran,* vol. 10, no. 1, pp. 27-33, 2013.

[2] S. Mohan Kumar and N. S. Shanmugam, "Finite element simulation for tensile and impact test of activated TIG welding of AISI 321 austenitic stainless steel," *Proceedings of the Institution of Mechanical Engineers, Part L,* vol. 233, no. 11, pp. 2323-2334, 2019.

[3] L. Natrayan, R. Anand, and S. Santhosh Kumar, "Optimization of process parameters in TIG welding of AISI 4140 stainless steel using Taguchi technique," *Materials Today: Proceedings,* vol. 37, pp. 1550-1553, 2021.

[4] A. N. Chaudhari, K. Dixit, G. S. Bhatia, B. Singh, P. Singhal, and K. K. Saxena, "Welding behaviour of duplex stainless Steel AISI 2205: AReview," *Materials Today: Proceedings,* vol.18, pp. 2731-2737, 2019.

[5] T. S. Chern, K. H. Tseng, and H. L. Tsai, "Study of the characteristics of duplex stainless-steel activated tungsten inert gas welds," *Materials & Design,* vol. 32, no. 1, pp. 255-263, 2011.

[6] G. Venkatesan, J. George, M. Sowmyasri, and V. Muthupandi, "Effect of ternary fluxes on depth of penetration in A-TIG welding of AISI 409 ferritic stainless steel," *Procedia Materials Science,* vol. 5, pp. 2402-2410, 2014.

[7] K. H. Tseng, "Development and application of oxide-based flux powder for tungsten inert gas welding of austenitic stainless steels," *Powder Technology,* vol. 233, pp. 72-79, 2013.

[8] A. K. Unni and M. Vasudevan, "Numerical modelling of fluid flow and weld penetration in activated TIG welding," *Materials Today: Proceedings,* vol. 27, pp. 2768-2773, 2020.

[9] S. Tathgir, D. W. Rathod, and A. Batish, "A-TIG welding process for enhanced-penetration in Duplex stainless-steel: effect of activated fluxes," *Materials and Manufacturing Processes,* vol. 34, no. 15, pp. 1659-1670, 2019.

[10] A. K. Unni, and V. Muthukumaranv, "Numerical simulation of the influence of oxygen content on the weld pool depth during activated TIG welding," *The International Journal of Advanced Manufacturing Technology,* vol.112 no. 1 ,pp. 467-489, 2021.

[11] A. R. Kohandehghan, S. Serajzadeh, and A. H. Kokabi, "A study on residual stresses in gas tungsten arc welding of AA5251," *Materials and Manufacturing Processes,* vol. 25, no. 11, pp. 1242-1250, 2010.

[12] K. C. Ganesh *et al.*, "Modeling, prediction and validation of thermal cycles, residual stresses and distortion in type 316 LN stainless steel weld joint made by TIG welding process," *Procedia Engineering,* vol. 86, pp. 767-774, 2014.

[13] D. Deng, "FEM prediction of welding residual stress and distortion in carbon steel considering phase transformation effects," *Materials & Design*, vol. 30, no. 2, pp. 359-366, 2009.

[14] A. S. Ahmad, Y. Wu, H. Gong, and L. Nie, "Finite element prediction of residual stress and deformation induced by double-pass TIG welding of Al 2219 plate," *Materials*, vol. 12, no. 14, p. 2251, 2019.

[15] D. Deng and H. Murakawa, "Prediction of welding distortion and residual stress in a thin plate butt-welded joint," *Computational Materials Science*, vol. 43, no. 2, pp. 353-365, 2008.

[16] P. Colegrove *et al.*, "Welding process impact on residual stress and distortion," *Science and Technology of Welding and Joining,* vol. 14, no. 8, pp. 717-725, 2009.

[17] P. Vasantharaja, V. Maduarimuthu, M. Vasudevan, and P. Palanichamy, "Assessment of residual stresses and distortion in stainless steel weld joints," *Materials and Manufacturing Processes,* vol. 27, no. 12, pp. 1376-1381, 2012.

[18] P. Vasantharaja, M. Vasudevan, and P. Palanichamy, "Effect of welding processes on the residual stress and distortion in type 316LN stainless steel weld joints," *Journal of Manufacturing Processes,* vol. 19, pp. 187-193, 2015.

[19] E. D. Derakhshan, N. Yazdian, B. Craft, S. Smith, and R. Kovacevic, "Numerical simulation and experimental validation of residual stress and welding distortion induced by laser-based welding processes of thin structural steel plates in butt joint configuration," *Optics & Laser Technology,* vol. 104, pp. 170-182, 2018.

[20] V. García-García, I. Mejía, F. Reyes-Calderón, J. A. Benito, and J. M. Cabrera, "FE thermo-mechanical simulation of welding residual stresses and distortion in Ti-containing TWIP steel through GTAW process," *Journal of Manufacturing Processes*, vol. 59, pp. 801-815, 2020.

[21] J. Chen *et al.*, "An experimental and numerical analysis of residual stresses in a TIG weldment of a single crystal nickel-base superalloy," *Journal of Manufacturing Processes,* vol. 53, pp. 190-200, 2020.

[22] J. Sun, J. Klassen, T. Nitschke-Pagel, and K. Dilger, "Effects of heat source geometric parameters and arc efficiency on welding temperature field, residual stress, and distortion in thin-plate full-penetration welds," *The International Journal of Advanced Manufacturing Technology*, vol. 99, no.1, pp. 497-515, 2018.

[23] M. Zubairuddin, S. K. Albert, S. Mahadevan, M. Vasudevan, V. Chaudhari, and V. K. Suri, "Experimental and finite element analysis of residual stress and distortion in GTA welding of modified 9Cr-1Mo steel," *Journal of Mechanical Science and Technology,* vol. 28, no. 12, pp. 5095-5105, 2014.

[24] M. Farhang, O, Sam-Daliri, M. R. Farahani, and A. Vatani, "Effect of friction stir welding parameters on the residual stress distribution of Al-2024-T6 alloy," *Journal of Mechanical Engineering and Sciences,* vol. 15, no. 1, pp. 7684-7694, 2021.

[25] S. Gao, S. Geng, P. Jiang, G. Mi, C. Han, and L. Ren, "Numerical analysis of the deformation behavior of 2205 duplex stainless steel TIG weld joint based on the microstructure and micro-mechanical properties," *Materials Science and Engineering A,* vol. 815, p. 141303, 2021.

[26] M. Hashemzadeh, Y. Garbatov, and C. G. Soares, "Analytically based equations for distortion and residual stress estimations of thin butt-welded plates," *Engineering Structures,* vol. 137, pp. 115-124, 2017.

[27] B. Varbai and K. Májlinger, "Physical and theoretical modeling of the nitrogen content of duplex stainless-steel weld metal: Shielding gas composition and heat input effects," *Metals*, vol. 9, no. 7, p. 762, 2019.

[28] M. Jurica, Z. Kožuh, I. Garašić, and M. Bušić, "Optimization of the A-TIG welding for stainless steels," *IOP Conference Series: Materials Science and Engineering*, vol. 329, 2018.

[29] Y. Chen, B. Yang, Y. Zhou, Y. Wu, and H. Zhu, "Evaluation of pitting corrosion in duplex stainless steel Fe20Cr9Ni for nuclear power application," *Acta Materialia,* vol. 197, pp. 172-183, 2020.

[30] A. Mahajan, S. S. Sidhu, and S. Devgan, "Examination of hemocompatibility and corrosion resistance of electrical discharge-treated duplex stainless steel (DSS-2205) for biomedical applications," *Applied Physics A,* vol. 126, no. 9, pp. 1-11, 2020.

[31] V. D. Kalyankar and G. P. Chudasama, "Influence of electrode tip diameter on metallurgical and mechanical aspects of spot welded duplex stainless steel," *High Temperature Materials and Processes,* vol. 39, no. 1, pp. 317-327, 2020.

[32] A. K. Maurya, C. Pandey, and R. Chhibber, "Dissimilar welding of duplex stainless steel with Ni alloys: A review," *International Journal of Pressure Vessels and Piping*, vol. 192, p. 104439, 2021.

[33] S. Madhankumar, K. Manonmani, V. Karthickeyan, and N. Balaji, "Optimization of ultimate tensile strength of welded Inconel 625 and duplex 2205," *Journal of Mechanical Engineering and Sciences*, vol. 15, no. 1, pp. 7715-7728, 2021.

[34] G. Magudeeswaran, S. R. Nair, L. Sundar, and N. Harikannan, "Optimization of process parameters of the activated tungsten inert gas welding for aspect ratio of UNS S32205 duplex stainless-steel welds," *Defence Technology*, vol. 10, no. 3, pp. 251-260, 2014.

[35] A. I. Mourad, A. Khourshid, and T. Sharef, "Gas tungsten arc and laser beam welding processes effects on duplex stainless steel 2205 properties," *Materials Science and Engineering A*, vol. 549, pp. 105-113, 2012.

[36] N. N. Korra, M. Vasudevan, and K. R. Balasubramanian, "Multi-objective optimization of activated tungsten inert gas welding of duplex stainless-steel using response surface methodology," *The International Journal of Advanced Manufacturing Technology*, vol. 77, no. 1, pp. 67-81, 2015.

[37] K. N. Naik, K. Balasubramanian, and M. Vasudevan, "Finite element simulation of A-TIG welding of duplex stainless steel 2205 using SYSWELD," *Applied Mechanics and Materials*, vol. 592, pp. 374-379, 2014.

[38] B. Brickstad and B. L. Josefson, "A parametric study of residual stresses in multi-pass butt-welded stainless steel pipes," *International Journal of Pressure Vessels and Piping*, vol. 75, no. 1, pp. 11-25, 1998.

[39] C. R. Xavier, H. G. Delgado, and J. A. d. Castro, "An experimental and numerical approach for the welding effects on the duplex stainless-steel microstructure," *Materials Research*, vol. 18, pp. 489-502, 2015.

[40] Ø. Grong, *Metallurgical Modelling of Welding*. Institute of Materials, 1997.

[41] M. Slováček, V. Diviš, L. Junek, V. Ochodek, "Numerical simulation of the welding process—distortion and residual stress prediction, heat source model determination," *Welding in the World*, vol. 49, no. 11, pp. 15-29, 2005.

[42] K. D. Ramkumar *et al.*, "Investigations on structure–property relationships of activated flux TIG weldments of super-duplex/austenitic stainless steels," *Materials Science and Engineering A*, vol. 638, pp. 60-68, 2015.

[43] M. Eftekhari, M. Ahmadi Najaf Abadi, and M. Farahani, "Evaluation of longitudinal residual stress variations along the thickness of welded joint of 5086 aluminum alloy," *Journal of Solid and Fluid Mechanics*, vol. 7, no. 3, pp. 1-16, 2017.

[44] C. Liu, Y. Luo, M. Yang, and Q. Fu, "Three-dimensional finite element simulation of welding residual stress in RPV with two J-groove welds," *Welding in the World*, vol. 61, no. 1, pp. 151-160, 2017.

[45] F. A. Kandil, J. D. Lord, A. T. Fry, and P. V. Grant, "A review of residual stress measurement methods-a guide to technique selection," NPL Report MATC(A)O4, National Physical Laboratory, Middlesex, UK, 2001.